Analysis of New Measurements of 18O-substituted Isotopic Species 16O16O18O and 16O18O16O of Ozone in the THz and Far-Infrared Ranges

E. Starikova, A. Barbe, L. Manceron, B. Grouiez, J. Burgalat, V. Tyuterev

ISSN 1024-8560, Atmospheric and Oceanic Optics, 2024, Vol. 37, No. 2, pp. 132–141. © The Author(s), 2024. This article is an open access publication.
Russian Text © The Author(s), 2024, published in Optika Atmosfery i Okeana.

SPECTROSCOPY OF AMBIENT MEDIUM

Analysis of New Measurements of ^{18}O-substituted Isotopic Species $^{16}O^{16}O^{18}O$ and $^{16}O^{18}O^{16}O$ of Ozone in the THz and Far-Infrared Ranges

E. N. Starikova[a, b, *], A. Barbe[c], L. Manceron[d, e], B. Grouiez[c], J. Burgalat[c], and V. G. Tyuterev[a, b]

[a] *V.E. Zuev Institute of Atmospheric Optics SB RAS, Tomsk, 634055 Russia*

[b] *Tomsk State University, Tomsk, 634050 Russia*

[c] *Groupe de Spectrométrie Moléculaire et Atmosphérique, UMR CNRS 7331, UFR Sciences Exactes et Naturelles, Reims Cedex 2, BP 1039-51687 France*

[d] *Synchrotron SOLEIL, Beamline AILES, Saint-Aubin, 91190 France*

[e] *Laboratoire Interuniversitaire des Systèmes Atmosphériques (LISA) UMR CNRS 7583, Créteil Cedex, 94010 France*

**e-mail: starikova_e@iao.ru*

Received October 20, 2023; revised November 14, 2023; accepted November 15, 2023

Abstract—High-resolution spectra corresponding to the rotational and the ν_2–ν_2 bands of the two most abundant isotopic species of ozone with one heavy ^{18}O oxygen atom were recorded using SOLEIL synchrotron radiation source in the range 30–200 cm^{-1}. Additionally, the ν_2 vibrational-rotational bands were recorded between 550 and 880 cm^{-1} using a classical glowbar source that made it possible to extend and refine information compared to published data on the observed transitions of these bands. The analyses of recorded spectra permitted us to deduce experimental set of energy levels for the ground (000) and the first bending (010) vibrational states, which significantly exceeds literature data in terms of rotational quantum numbers. For both isotopic species, the weighted fits of all experimental line positions were carried out including previously published microwave data. As a result of this work, the improved values of rotational and centrifugal distortion parameters for the states (000) and (010) were obtained that permitted modelling the experimental line positions with a weighted standard deviation of 1.284 (2235 transitions) and 0.908 (4597 transitions), respectively, for $^{16}O^{16}O^{18}O$, and 1.168 (824 transitions) and 1.724 (2381 transitions) for $^{16}O^{18}O^{16}O$.

Keywords: ozone, isotopic modification, effective Hamiltonian model, rotational band, ν_2–ν_2 and ν_2 bands

DOI: 10.1134/S1024856024700167

INTRODUCTION

The ozone molecule, which absorbs the light nearly everywhere from the microwave (MW) to the infrared (IR) and ultra-violet ranges [1–4], plays the major role in the atmospheric physics and chemistry with an impact on climate, ecosystems and human health. One of incentives for the study of absorption spectra of the isotopically substitutes ozone was a discovery of isotopic anomalies in atmospheric conditions and laboratory experiments [5–8]. Another one is the experimental validation of *ab initio* potential energy surfaces (PES) which are used for the modeling of the ozone formation [9] and isotopic exchange reactions [10–12].

After the main isotopic species of ozone $^{16}O_3$, its most abundant isotopomers are $^{16}O^{16}O^{18}O$ and $^{16}O^{18}O^{16}O$ with the statistical natural abundances of 0.00389 and 0.00199 correspondingly [13]. Available information for the line lists are collected in HITRAN [14], GEISA [15], and S&MPO (Spectroscopy and Molecular Properties of Ozone) [13] databases partly accessible via European VAMDC portal [16]. Analyses of infrared spectra of these species measured with Fourier Transform Spectroscopy (FTS) techniques were reported in [17–21], whereas spectra at higher energy ranges measured with Cavity-ring-down Spectroscopy (CRDS) techniques were reported in [22–24].

Ozone has a large permanent dipole moment and exhibits a strong absorption in the MW, THz and far-infrared (FIR) range corresponding to the ν_2 fundamental band. For the purely rotational bands of $^{16}O^{16}O^{18}O$ and $^{16}O^{18}O^{16}O$ only quite sparse but very accurate measurements have been reported by Depannemaecker [25] and Chiu [26] using microwave techniques. For the ν_2 band, the previous FTS measurements have been published by Flaud et al. [27].

The aim of this work is to report the results of the analysis of two new series of experimental FTS spectra recorded with the experimental SOLEIL equipment [28–30] of the CNRS (National Center of Scientific

Table 1. Summary of the experimental conditions

Spectrum No.	Total ozone pressure, Torr	Optical path, cm	Temperature, K	Path difference, cm	$^{16}O_2$, %	$^{18}O_2$, %	Resolution, cm^{-1}
d20318.3	1.725	816	296.15	450.00	62.50	37.50	0.002
d20326.1	2.376	280	295.80	882.35	47.93	52.07	0.001

Research of France) and of their simultaneous treatment with available microwave data [25, 26].

The longwave range between 1.2–6 THz (30–200 cm^{-1}) spectra were recorded using Synchrotron light source of the SOLEIL setup that permitted to measure a large number of rotational lines including "hot" bands, due to the exceptional brightness of the Synchrotron radiation, sensitivity of measurements and improved signal-to-noise ratio. For the ν_2 band, the supplementary measurements were carried out with better spectral resolutions that the previously available ones [27].

1. EXPERIMENT

The experimental setup of measurements of ozone spectra using SOLEIL CNRS equipment has been described by Manceron et al. [31, 32]. Here, we only summarize the main features of the experiments. Some more technical details can be found in the work [33] devoted to the study of the principle isotopologue $^{16}O_3$, which was using a similar setup.

The ozone was synthesized using electric discharge from batches of 7 to 20 Torr of high purity oxygen (99.9995%) and heavy ^{18}O-labelled oxygen (99% ^{18}O). Mixtures using different proportions of the diatomic oxygen $^{16}O_2 + {}^{18}O_2$ produced then six isotopic forms of ozone $^{16}O_3$, $^{16}O^{16}O^{18}O$, $^{16}O^{18}O^{16}O$, $^{16}O^{18}O^{18}O$, $^{18}O^{16}O^{18}O$ and $^{18}O_3$, which for brevity will be denoted using simplified commonly used 666, 668, 686, 688, 868 and 888 labels.

As outlined in the Introduction, two series of experimental spectra were recorded with two different mixtures of ^{18}O enriched ozone isotopomers. Both of them were recorded using a Bruker IFS125HR Fourier transform spectrometer.

For the first series of experiments in the range 1.2–6 THz (30–200 cm^{-1}), the spectrometer was linked to the AILES Beamline at the Synchrotron SOLEIL setup [28–30].The maximum optical path difference (MOPD) was set to 450 cm (giving a sinc function width of about 0.00134 cm^{-1}). The Synchrotron source was operated with 500 mA in the most stable, multibunch mode and the synchrotron effective source size is compatible with the highest resolution over the whole spectral domain [30]. For this first series of measurement in the terahertz range the ozone isotopic species were generated from a $^{16}O_2$ (62.5%) + $^{18}O_2$ (37.5%) mixture giving the total ozone pressure of 1.725 Torr with the optical pathlength of 816 cm.

The second series was carried out at higher wavenumber range between 550 and 880 cm^{-1} using classical glowbar source with a 1.3 mm entrance iris diameter. The MOPD was set to 882 cm, giving a sinc function width of about 0.00068 cm^{-1}. Table 1 gives the summary of the experimental conditions. An overview of analyzed spectra with demonstration on small areas of 0.3 cm^{-1} width is shown in Fig. 1.

The spectra were calibrated with residual CO_2 lines observed in the spectrum with their wavenumbers taken from HITRAN [14]. The resulting accuracy is ± 0.00005 cm^{-1} for well isolated lines. In this experiment for the ν_2 band region, the optical path length was set to 2.8 m ozone (spectrum d20326.1) and the total pressure, generated from a $^{16}O_2$ (47.93%) + $^{18}O_2$ (52.07%) mixture giving the total was 2.376 Torr.

2. ANALYSIS AND MODELLING

To work with these spectra, we have used the following programs: MultiFit [34] to visualize experimental and calculated spectra and determine the positions of experimental lines using graphical peak-finder tools; and ASSIGN [35] to identify series of transitions to the same vibrational-rotational (VR) level using combinational differences. The series of VR transitions were calculated with the computational code GIP [36] for both symmetry groups C_S and C_{2V}. Identification was carried out iteratively, series by series, as the quantum numbers J and K_a increased, using extrapolation based on an initial effective Hamiltonian model.

The effective Hamiltonian (H^{eff}) in the representation of rotation operators described in [37] (and references therein) was used to fit experimental data:

$$H^{\text{eff}} = \sum_{lm} b_{Lm0}\mathbf{J}^{2l}J_z^m + \sum_{lm} b_{Lm2}\mathbf{J}^{2l}\left\{J_+^2(J_z+1)^m + (J_z+1)^m J_-^2\right\}, \quad (1)$$

where J_z is the component of the angular momentum along the A-axis in I^r representation [38] and $J_\pm$ are the ladder combinations of J_x, J_y components in the molecular Eckart frame, and $\mathbf{J}^2$ is the square of the total angular momentum with the low case index notation $L = 2l$.

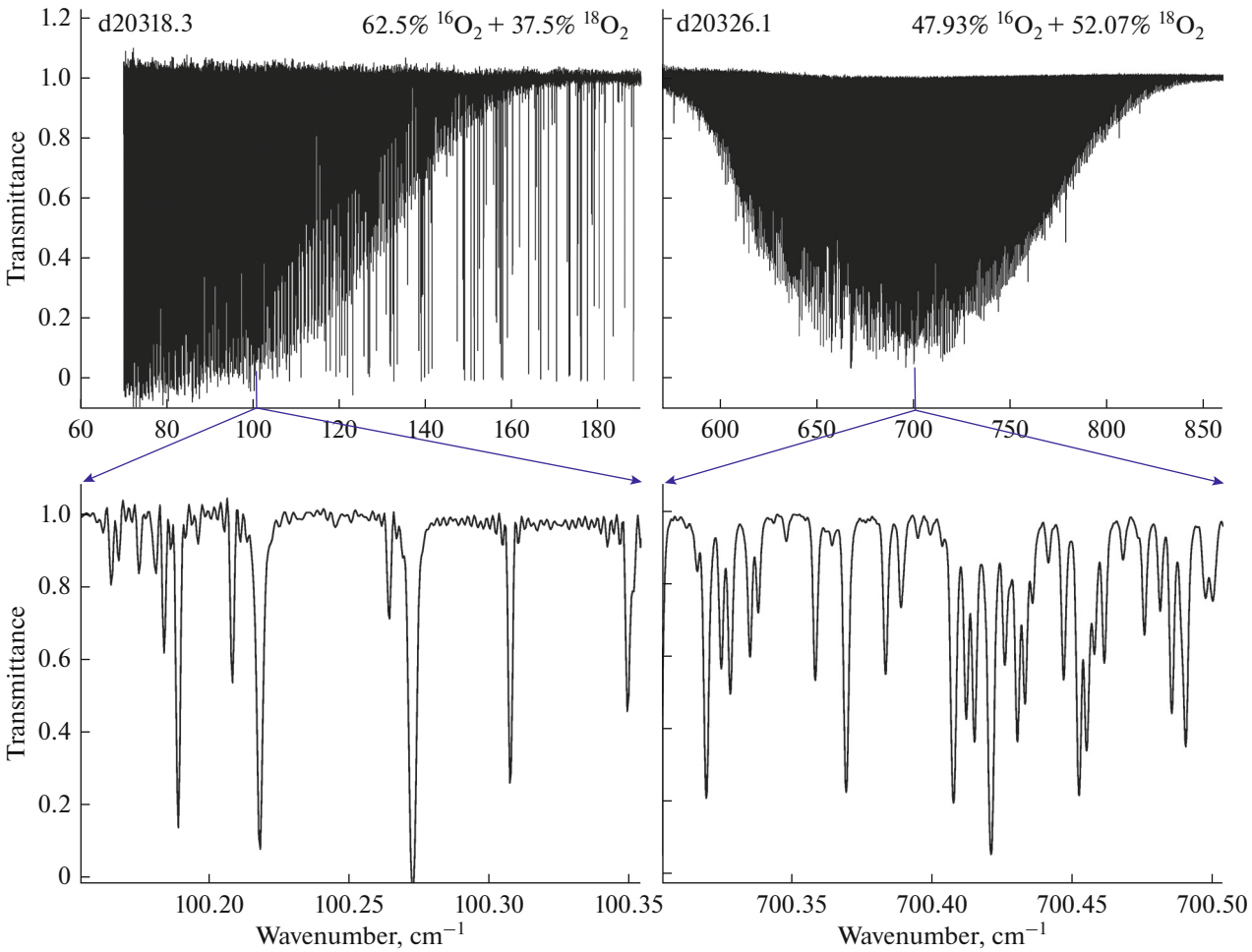

Fig. 1. Overview of the spectra of ozone enriched with oxygen ^{18}O recorded using SOLEIL setup.

In this work, we did not proceed to the intensity measurement of experimental lines to refine the parameters of the effective dipole transition moments [39, 40]. Previously published effective parameters of the dipole transition moment of the bands {(000)–(000), (010)–(010), (010)–(000)} from the S&MPO database [13] were used to calculate the synthetic spectra and evaluate the correctness of the identification performed using the MultiFit program of the studied isotopic species of ozone.

Spectroscopic parameters of the ground and first excited vibrational states of the ozone isotopomers $^{16}O^{16}O^{18}O$ and $^{16}O^{18}O^{16}O$ were previously obtained by Flaud et al. in [27]. The authors of [27] analyzed Fourier spectra in the range of the ν_2 band recorded in 1985 at room temperature with a resolution of 0.005 cm^{-1} using the McMath solar telescope complex at Kitt Peak National Observatory. Note that this paper [27] did not contain information about the set of experimental data which had been obtained from the analysis of the band ν_2, including the number of VR transitions and the maximum values of rotational quantum numbers. It was only pointed out that for identifying and modelling series of transitions with $K_a > 11$, they carried out simultaneous processing IR and microwave data [25] in order to improve parameters of the ground state (000). As a result of the modelling, they obtained the parameters of the effective Watson Hamiltonian [41] to calculate the line lists [42] for the ν_2 bands up to the maximum values of $J = 65$, $K_a = 17$ and $E_{max} = 1750$ cm^{-1}. Their intensity cut off was 0.25×10^{-22} and 0.50×10^{-22} cm/molec at 296 K for $^{16}O^{16}O^{18}O$ and $^{16}O^{18}O^{16}O$, respectively. The calculated lists were included in the HITRAN and S&MPO databases, and the obtained ground state parameters were taken as "reference" ones when analysing all the following bands and for corresponding calculations.

The spectra recorded in the range of 30–200 cm^{-1} with the SOLEIL synchrotron facility allowed us to expand the set of experimentally observed rotational transitions of the bands (000)–(000) and (010)–(010) for each isotopic modification with respect to the line lists available in the databases. Graphically, this comparison is presented in Figs. 2a, 2c and 3a, 3c for

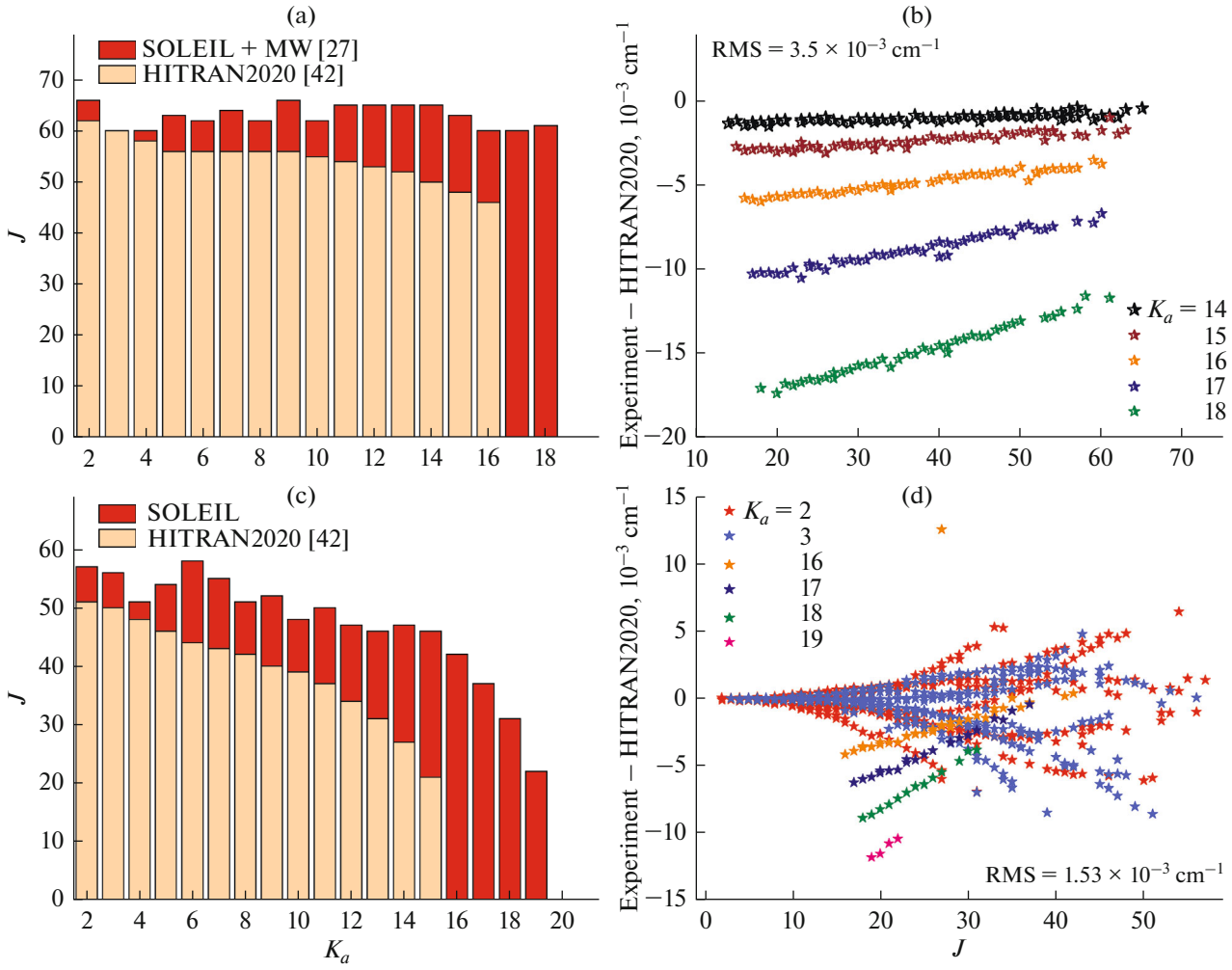

Fig. 2. A comparative diagram of the maximum rotational quantum numbers J and K_a for the $^{16}O^{16}O^{18}O$ bands (000)–(000) (a) and (010)–(000) (c) experimentally observed in our work versus the HITRAN2020 line lists [14], which have been calculated using the parameters [27]; the differences between the observed line positions of the (000)–(000) (b) and (010)–(000) (d) bands and the HITRAN2020 data.

$^{16}O^{16}O^{18}O$ and $^{16}O^{18}O^{16}O$, respectively. In addition, the comparison shows a significant discrepancy between the positions of our experimental lines versus HITRAN2020, particularly for transitions with high J and K_a values (Figs. 2b, 2d and 3b, 3d). For example, despite a small standard deviation (*RMS*) equal to 1.53×10^{-3} cm^{-1} for the band ν_2 $^{16}O^{16}O^{18}O$, the difference in the positions of the HITRAN2020 lines from the experimental ones for transitions with $K_a = 19$ reaches 11.8×10^{-3} cm^{-1}.

2.1. Isotopomer $^{16}O^{16}O^{18}O$

With the initial parameters of Flaud et al. [27] it was possible to identify purely rotational transitions of the ground state in the spectrum of d20318.3 for small values of quantum numbers up to $J = 25$ and $K_a = 8$. By adjusting the H^{eff} parameters iteratively in the modelling process we were able to identify 2051 transitions of this band up to $J = 67$ and $K_a = 18$. The parameters obtained in the weighted fit of experimental transition frequencies together with microwave data [25] allowed us to model rotational microwave transitions of the band (000)–(000) with a standard deviation of 0.2×10^{-5} cm^{-1}. This includes the fit of experimental transitions measured in our work with $RMS = 0.171 \times 10^{-3}$ cm^{-1}, and the entire set of transitions with weighted standard deviation of 1.284 (Table 2).

At the next stage, we fixed the obtained parameters of the ground state and varied only the parameters of the (010) bending state during the simultaneous fit of three data sets. These sets include the rotational transitions ν_2–ν_2 obtained from the microwave spectra [26] and the SOLEIL spectrum (d20318.3) in the range of 30–200 cm^{-1}, as well as VR transitions of the ν_2 band assigned in the range of 550–880 cm^{-1} in the

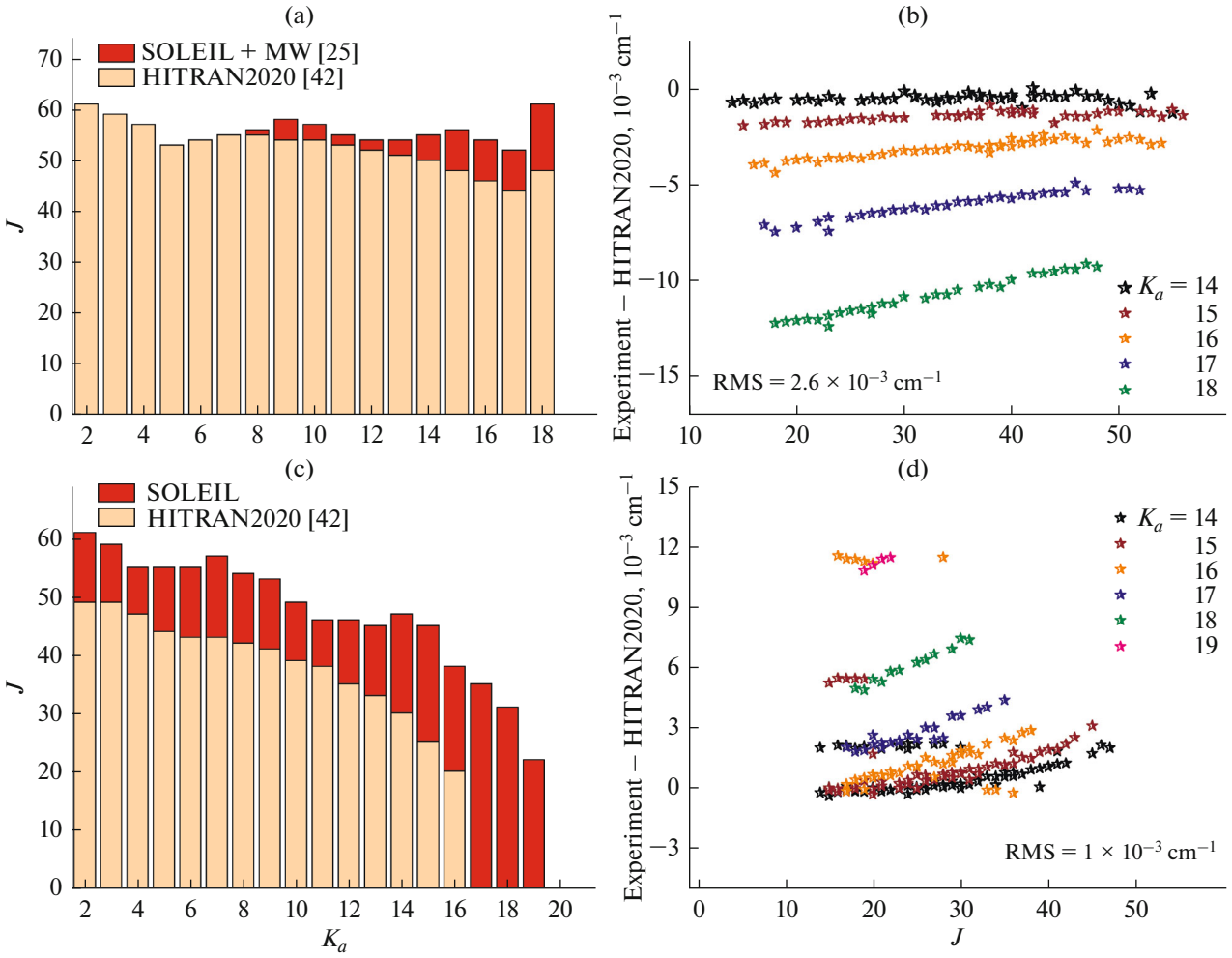

Fig. 3. Same as in Fig. 2, but for $^{16}O^{18}O^{16}O$.

Table 2. Overall statistics of experimental transitions of $^{16}O^{18}O^{16}O$ and $^{16}O^{16}O^{18}O$ ozone isotopomers included in the simultaneous fit. Treatment results

	Bande/Source	Nb Tran	J_{max}	$K_{a_{max}}$	*RMS*, 10^{-3} cm^{-1}	Weighted standard deviation
668	000–000 SOLEIL*	2051	67	18	0.171	1.284
	000–000 MW [25]	184	43	7	0.002	
	010–010 SOLEIL*	348	41	17	0.142	0.908
	010–010 MW [26]	56	46	7	0.002	
	010–000 SOLEIL**	4193	63	19	0.114	
686	000–000 SOLEIL*	729	62	18	0.155	1.168
	000–000 MW [25]	95	39	6	0.002	
	010–010 SOLEIL*	113	39	17	0.162	1.724
	010–010 MW [26]	39	48	8	0.008	
	010–000 SOLEIL**	2229	61	19	0.165	

* Spectrum recorded in the range of 30–200 cm^{-1} on a Bruker IFS125HR spectrometer connected to the AILES source of the SOLEIL synchrotron setup.
** Spectrum recorded in the range of 550–880 cm^{-1} using Bruker IFS125HR with the glowbar source.

Table 3. Spectroscopic parameters of H^{eff} for the (000) and (010) states of the $^{16}O^{18}O^{16}O$ and $^{16}O^{16}O^{18}O$ ozone isotopomers, obtained in a simultaneous fit of the observed line positions in the MW, FIR and THz ranges

(1)	(*)		(686)		(668)	
			(000)	(010)	(000)	(010)
b_{000}	E^{VV}		0.000	693.305613_2 (12)	0.000	684.613331_6 (58)
b_{020}	$A-(B+C)/2$		2.87213509_3 (26)	2.92501165_4 (28)	3.09117656_3 (20)	3.14279177_7 (14)
b_{200}	$(B+C)/2$		0.418364426_1 (43)	0.416544712_4 (37)	0.397008624_9 (29)	0.395384678_9 (17)
b_{002}	$(B-C)'/4$		0.0135142786_5 (29)	0.0138181416_6 (42)	0.0114969275_8 (17)	0.0117187662_4 (15)
$-b_{040}$	Δ_K	$\times10^3$	0.1809645_8 (70)	0.1992172_7 (40)	0.2039657_0 (45)	0.2235790_4 (24)
$-b_{220}$	Δ_{JK}	$\times10^5$	-0.13190_9 (10)	-0.123432_0 (56)	-0.190523_7 (38)	-0.186315_9 (20)
$-b_{400}$	Δ_J	$\times10^6$	0.447859_1 (57)	0.451225_0 (31)	0.406902_5 (26)	0.409308_0 (14)
$-b_{202}$	δ'_J	$\times10^7$	0.729210_5 (95)	0.723139_8 (75)	0.606036_6 (43)	0.602170_8 (30)
$-b_{022}$	δ'_K	$\times10^5$	0.310612_1 (92)	0.36994_7 (17)	0.291253_7 (64)	0.349231_2 (67)
b_{060}	H_K	$\times10^7$	0.31519_7 (34)	0.39597_9 (26)	0.37337_2 (24)	0.46036_2 (14)
b_{240}	H_{KJ}	$\times10^8$	-0.15245_8 (78)	-0.15870_8 (50)	-0.16417_4 (41)	-0.18975_0 (24)
b_{420}	H_{JK}	$\times10^{10}$	0.111_0 (13)	-0.080_2 (11)	-0.1577_0 (73)	-0.0759_1 (43)
b_{600}	H_J	$\times10^{12}$	0.396_4 (15)	0.4334_2 (72)	0.2812_6 (59)	0.2525_3 (32)
b_{042}	h'_K	$\times10^8$	0.1658_7 (85)	0.2089_9 (79)	0.1507_3 (70)	0.23959_4 (40)
b_{222}	h'_{JK}	$\times10^{11}$		-0.565_5 (68)		-0.342_8 (28)
b_{402}	h'_J	$\times10^{12}$	0.1760_8 (54)	0.1929_9 (23)	0.1156_5 (17)	0.12843_6 (99)
b_{080}	L_K	$\times10^{11}$	-0.9017_2 (62)	-1.4367_2 (47)	-1.0506_6 (44)	-1.6046_8 (24)
b_{260}	L_{KKJ}	$\times10^{12}$	0.355_5 (15)		0.2894_8 (65)	0.4551_9 (60)
b_{440}	L_{JK}	$\times10^{13}$	-0.141_7 (18)	-0.226_1 (17)		
b_{0100}	P_K	$\times10^{14}$	0.348 [f]	0.711 [f]	0.348 [f]	0.711 [f]

[f] fixed to the values of $^{16}O_3$ [33]; (*) definition of the parameters in model (1): the diagonal rotational terms have the same form as in the Watson model [41]; the primes indicate that slight differences occur between the definition of parameters in Eq. (1) and the original Watson definition accounting for the $[J_+, J_z]$ commutation relations. The statistical standard deviations of the parameters obtained by the least squares method are given in parentheses.

spectrum d20326.1. The final set of the (010) state parameters for the isotopomer $^{16}O^{16}O^{18}O$, given in Table 3, permitted modelling the entire set of 4597 transitions with a weighted standard deviation of 0.908.

2.2. Isotopomer $^{16}O^{18}O^{16}O$

The lines of the isotopomer $^{16}O^{18}O^{16}O$ were identified using a similar procedure. In total, 729 purely rotational ground state transitions up to $J = 62$ and $K_a = 18$ were identified in the spectra studied in our work. Despite the fact that the information obtained on the J_{max} and $K_{a_{max}}$ only slightly exceeds the set of quantum numbers of this band in HITRAN2020 (Fig. 3a), the difference between the line positions of the experimental transitions and those calculated in HITRAN2020 increases with increasing energy and reaches 12.5×10^{-3} cm^{-1} for the $K_a = 18$ series (Fig. 3b). Using the simultaneous fit with microwave data [27], we obtained a weighted standard deviation of 1.168.

For the ν_2 band, the set of vibrational-rotational transitions was significantly expanded compared to published literature data (Fig. 3c): in total, 2229 transitions of the ν_2 band up to $J = 61$ and $K_a = 19$ were identified in the spectrum. Their simultaneous fit (Table 2) with the transitions of the hot band ν_2–ν_2 obtained from the SOLEIL spectra in our work and with the microwave spectra [26] permitted to obtain more accurate set of effective Hamiltonian parameters for $^{16}O^{18}O^{16}O$ given in Table 3.

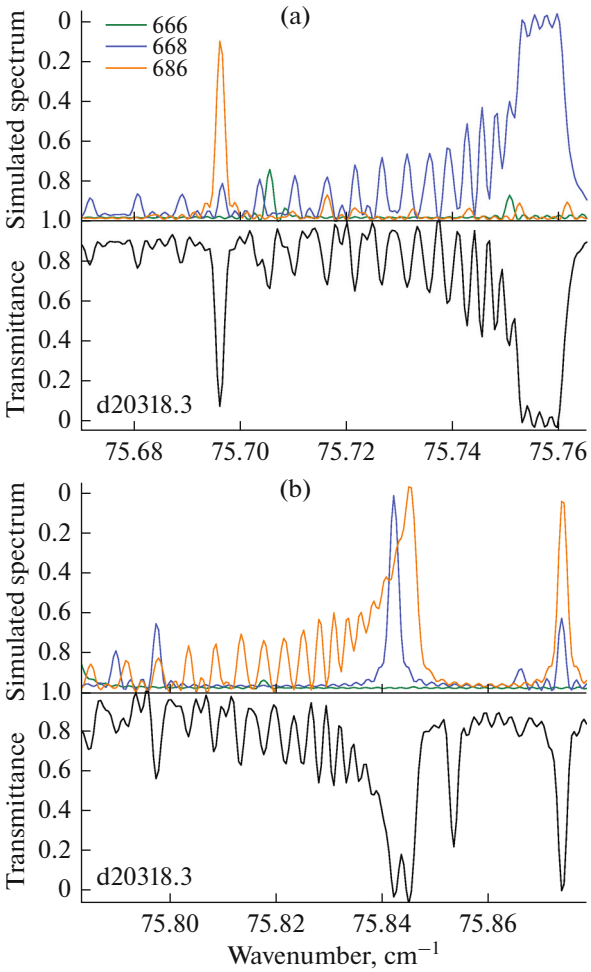

Fig. 4. Comparison of the experimental ozone spectrum (d20318.3) recorded using the SOLEIL synchrotron setup with the calculated spectrum in the region of 75.8 cm^{-1}. The left-hand panel (a) shows an example of the dominant contribution of the *Q*-branch rotational band of the isotopomer $^{16}O^{16}O^{18}O$, the right-hand panel (b) – of the isotopomer $^{16}O^{18}O^{16}O$.

3. RESULTS

The detailed line statistics of the $^{16}O^{18}O^{16}O$ and $^{16}O^{16}O^{18}O$ ozone isotopomers assigned in the SOLEIL spectra, as well as the MW data [25, 26], included in the simultaneous fit are collected in Tables 2. The resulting parameters of the (000) and (010) states are presented in Table 3.

Using the parameters of the effective Hamiltonians of the (000) and (010) states obtained in our work, as well as the parameters of the effective dipole moments of the bands from the S&MPO database [13], the lists of lines for $^{16}O^{18}O^{16}O$ and $^{16}O^{16}O^{18}O$, including transitions (000)–(000), (010)–(000), and (010)–(010) were calculated. The partition function *Q(T)* was taken [13] equal 7565.675 and 3647.080 for $^{16}O^{16}O^{18}O$ and $^{16}O^{18}O^{16}O$, respectively. The calculated spectra

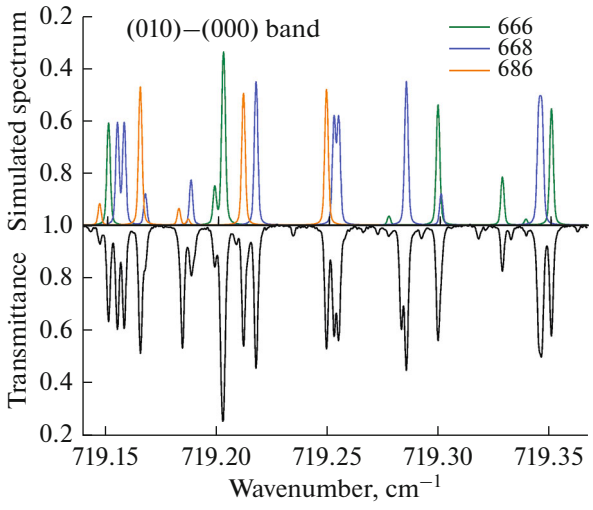

Fig. 5. Comparison of the experimental spectrum of ozone (d20326.1) registered in the far- infrared range of about 719.2 cm^{-1} (low panel) with the calculated in this work spectrum (upper panel).

constructed using these lists gave good agreement with the experiment. Figs. 4 and 5 show such a comparison in the ranges 75.8 and 719.2 cm^{-1}, respectively.

The line lists for the main isotopic modification of ozone was taken from the work [33] devoted to the study of $^{16}O_3$ spectra recorded at SOLEIL. In the future, it is planned to perform theoretical calculations of line intensities using ab initio dipole moment [43].

CONCLUSIONS

The FTS spectra of ozone isotopically enriched with oxygen ^{18}O recorded using the light source of AILES Beamline facility of the SOLEIL synchrotron in the range 1–6 THz (30–200 cm^{-1}), combined with new experimental spectra of the ν_2 bands recorded using glowbar source in the far-infrared range (550–880 cm^{-1}), allowed us to significantly expand the set of observed VR transitions up to $J_{max} = 67$, $K_{a_{max}} = 19$. As a result of their simultaneous fit with MW transitions, new parameters of the effective Hamiltonian of the states (000) and (010) of the isotopomers $^{16}O^{16}O^{18}O$ and $^{16}O^{18}O^{16}O$ were obtained. The accuracy of calculated spectra with the obtained parameters was significantly improved compared to the previously used reference parameters of J.M. Flaud et al. [27].

In the future work, we plan to use the obtained parameters, as well as theoretical calculations of line intensities using ab initio dipole moment to construct complete transition line lists for the studied bands and to fill the spectroscopy databases HITRAN, GEISA, S&MPO.

ACKNOWLEDGMENTS

The authors thank CNRS SOLEIL (France) for support of the experimental setup (project no. 20211156).

FUNDING

The work was supported by the Russian Science Foundation (project no. 19-12-00171-P).

CONFLICT OF INTEREST

The authors of this work declare that they have no conflicts of interest.

REFERENCES

1. S. Y. Grebenshchikov, Z. W. Qu, H. Zhu, and R. Schinke, "New theoretical investigations of the photodissociation of ozone in the Hartley, Huggins, Chappuis, and Wulf bands," Phys. Chem. Chem. Phys. **9**, 2044–2064 (2007). https://doi.org/10.1039/B701020F
2. J. Orphal, J. Staehelin, J. Tamminen, G. Braathen, M. R. De Backer, A. Bais, D. Balis, A. Barbe, P. K. Bhartia, M. Birk, J. B. Burkholder, K. Chance, T. von Clarmann, A. Cox, D. Degenstein, R. Evans, J. M. Flaud, D. Flittner, S. Godin-Beekmann, V. Gorshelev, A. Gratien, E. Hare, C. Janssen, E. Kyrola, T. McElroy, R. McPeters, M. Pastel, M. Petersen, I. Petropavlovskikh, B. Picquet-Varrault, M. Pitts, G. Labow, M. Rotger-Languereau, T. Leblanc, C. Lerot, X. Liu, P. Moussay, A. Redondas, M. Van Roozendael, S. P. Sander, M. Schneider, A. Serdyuchenko, P. Veefkind, J. Viallon, C. Viatte, G. Wagner, M. Weber, R. I. Wielgosz, and C. Zehner, "Absorption cross-sections of ozone in the ultraviolet and visible spectral regions: Status report 2015," J. Mol. Spectrosc. **327**, 105–121 (2016). https://doi.org/10.1016/J.JMS.2016.07.007
3. S. Vasilchenko, D. Mondelain, S. Kassi, and A. Campargue, "Predissociation and pressure dependence in the low frequency far wing of the Wulf absorption band of ozone near 1.2 μm," J. Quant. Spectrosc. Radiat. Transfer **278**, 107678 (2021). https://doi.org/10.1016/j.jqsrt.2021.107678
4. A. Barbe, S. Mikhailenko, E. Starikova, and V. Tyuterev, "High resolution infrared spectroscopy in support of ozone atmospheric monitoring and validation of the potential energy function," Molecules **27**, 911 (2022). https://doi.org/10.3390/MOLECULES27030911
5. M. H. Thiemens and J. E. Heidenreich, "The mass-independent fractionation of oxygen: A novel isotope effect and its possible cosmo chemical implications," Science **219**, 1073–1075 (1983).
6. K. Mauersberger, D. Krankowsky, C. Janssen, and R. Schinke, "Assessment of the ozone isotope effect," Adv. Atom. Mol. Optic. Phys. **50**, 1–54 (2005). https://doi.org/10.1016/S1049-250X(05)80006-0
7. Y. Q. Gao and R. A. Marcus, "Strange and unconventional isotope effects in ozone formation," Science **293**, 259–263 (2001).
8. J. M. Carlstad and K. A. Boering, "Isotope effects and the atmosphere," Ann. Rev. Phys. Chem. **74**, 439–465 (2023). https://doi.org/10.1146/annurev-physchem-061020-053429
9. M. Mirahmadi, J. Perez-Rios, O. Egorov, V. Tyuterev, and V. Kokoouline, "Ozone formation in ternary collisions: Theory and experiment doi," Phys. Rev. Lett. **128** (10), 108501 (2022). https://doi.org/10.1103/PhysRevLett.128.108501reconciled
10. C. Janssen, J. Guenther, D. Krankowsky, and K. Mauersberger, "Temperature dependence of ozone rate coefficients and isotope fractionation in ^{16}O–^{18}O oxygen mixtures," Chem. Phys. Lett. **367**, 34–38 (2003).
11. G. Guillon, P. Honvault, R. Kochanov, and V. Tyuterev, "First-principles computed rate constant for the $O + O_2$ isotopic exchange reaction now matches experiment," J. Phys. Chem. Lett. **9** (8), 1931–1936 (2018). doi . 9b06139 https://doi.org/10.1021/acs.jpca
12. C. H. Yuen, D. Lapierre, F. Gatti, V. Kokoouline, and V. G. Tyuterev, "The role of ozone vibrational resonances in the isotope exchange reaction $^{16}O^{16}O + {}^{18}O > {}^{18}O^{16}O + {}^{16}O$: The time-dependent picture," J. Phys. Chem. A **123** (36), 7733–7743 (2019).
13. Y. L. Babikov, S. N. Mikhailenko, A. Barbe, and V. G. Tyuterev, "S&MPO—an information system for ozone spectroscopy on the WEB," J. Quant. Spectrosc. Radiat. Transfer **145**, 169–196 (2014). https://doi.org/10.1016/j.jqsrt.2014.04.024
14. I. E. Gordon, L. S. Rothman, R. J. Hargreaves, R. Hashemi, E. V. Karlovets, F. M. Skinner, E. K. Conway, C. Hill, R. V. Kochanov, Y. Tan, P. Wcislo, A. A. Finenko, K. Nelson, P. F. Bernath, M. Birk, V. Boudon, A. Campargue, K. V. Chance, A. Coustenis, B. J. Drouin, J.-M. Flaud, R. R. Gamache, J. T. Hodges, D. Jacquemart, E. J. Mlawer, A. V. Nikitin, V. I. Perevalov, M. Rotger, J. Tennyson, G. C. Toon, H. Tran, V. G. Tyuterev, E. M. Adkins, A. Baker, A. Barbe, E. Cane, A. G. Csaszar, A. Dudaryonok, O. Egorov, A. J. Fleisher, H. Fleurbaey, A. Foltynowicz, T. Furtenbacher, J. J. Harrison, J.-M. Hartmann, V.-M. Horneman, X. Huang, T. Karman, J. Karns, S. Kassi,

I. Kleiner, V. Kofman, F. Kwabia-Tchana, N. N. Lavrentieva, T. J. Lee, D. A. Long, A. A. Lukashevskaya, O. M. Lyulin, V. Yu. Makhnev, W. Matt, S. T. Massie, M. Melosso, S. N. Mikhailenko, D. Mondelain, H. S. P. Muller, O. V. Naumenko, A. Perrin, O. L. Polyansky, E. Raddaoui, P. L. Raston, Z. D. Reed, M. Rey, C. Richard, R. Tobias, I. Sadiek, D. W. Schwenke, E. Starikova, K. Sung, F. Tamassia, S. A. Tashkun, Auwera J. Vander, I. A. Vasilenko, A. A. Vigasin, G. L. Villanueva, B. Vispoel, G. Wagner, A. Yachmenev, and S. N. Yurchenko, "The HITRAN2020 molecular spectroscopic database," J. Quant. Spectrosc. Radiat. Transfer **277**, 107949 (2022). https://doi.org/10.1016/j.jqsrt.2021.107949

15. T. Delahaye, R. Armante, N. A. Scott, N. Jacquinet-Husson, A. Chedin, L. Crepeau, C. Crevoisier, V. Douet, A. Perrin, A. Barbe, V. Boudon, A. Campargue, L. H. Coudert, V. Ebert, J.-M. Flaud, R. R. Gamache, D. Jacquemart, A. Jolly, TchanaF. Kwabia, A. Kyuberis, G. Li, O. M. Lyulin, L. Manceron, S. Mikhailenko, N. Moazzen-Ahmadi, H. S. P. Muller, O. V. Naumenko, A. Nikitin, V. I. Perevalov, C. Richard, E. Starikova, S. A. Tashkun, Vl. G. Tyuterev, Auwera J. Vander, B. Vispoel, A. Yachmenev, and S. Yurchenko, "The 2020 edition of the GEISA spectroscopic database," J. Mol. Spectrosc. **380**, 111510 (2021). https://doi.org/10.1016/j.jms.2021.111510

16. D. Albert, B. K. Antony, Y. A. Ba, Yu. L. Babikov, Ph. Bollard, V. Boudon, F. Delahaye, G. Del Zanna, M. S. Dimitrijevic, B. J. Drouin, M.-L. Dubernet, F. Duensing, M. Emoto, C. P. Endres, A. Z. Fazliev, J.-M. Glorian, I. E. Gordon, P. Gratier, C. Hill, D. Jevremovic, C. Joblin, D.-H. Kwon, R. V. Kochanov, E. Krishnakumar, G. Leto, P. A. Loboda, A. A. Lukashevskaya, O. M. Lyulin, B. P. Marinkovic, A. Markwick, T. Marquart, N. J. Mason, C. Mendoza, T. J. Millar, N. Moreau, S. V. Morozov, T. Moller, H. S. P. Muller, G. Mulas, I. Murakami, Yu. Pakhomov, P. Palmeri, J. Penguen, V. I. Perevalov, N. Piskunov, J. Postler, A. I. Privezentsev, P. Quinet, Yu. Ralchenko, Y.-J. Rhee, C. Richard, G. Rixon, L. S. Rothman, E. Roueff, T. Ryabchikova, S. Sahal-Brechot, P. Scheier, P. Schilke, S. Schlemmer, K. W. Smith, B. Schmitt, I. Yu. Skobelev, V. A. Sreckovic, E. Stempels, S. A. Tashkun, J. Tennyson, V. G. Tyuterev, Ch. Vastel, V. Vujciic, V. Wakelam, N. A. Walton, C. Zeippen, and C. M. Zwolf, "A decade with VAMDC: Results and ambitions," Atoms **8**, 76 (2020). https://doi.org/10.3390/atoms8040076

17. A. Barbe, S. Mikhailenko, E. Starikova, M.-R. De Backer-Barilly, Vl. G. Tyuterev, D. Mondelain, S. Kassi, A. Campargue, C. Janssen, S. Tashkun, R. Kochanov, R. Gamache, and J. Orphal, "Ozone spectroscopy in the electronic ground state: High resolution spectra analyses and update of line parameters since 2003," J. Quant. Spectrosc. Radiat. Transfer **130**, 172–190 (2013).

18. A. Barbe, E. Starikova, M.-R. De Backer, and Vl. G. Tyuterev, "Analyses of infrared spectra of asymmetric ozone isopotologue $^{16}O^{16}O^{18}O$ in the range 950–3850 cm^{-1}," J. Quant. Spectrosc. Radiat. Transfer **218**, 231–247 (2018).

19. E. Starikova, A. Barbe, M.-R. De Backer, and V. Tyuterev, "Analysis of thirteen absorption bands of $^{16}O^{18}O^{18}O$ ozone isotopomer in the 950–3500 cm^{-1} infrared spectral range," J. Quant. Spectrosc. Radiat. Transfer **257**, 107364 (2020).

20. A. Barbe, S. Mikhailenko, E. Starikova, and Vl. Tyuterev, "Infrared spectra of $^{16}O_3$ in the 900–5600 cm^{-1} range revisited: Empirical corrections to the S&MPO and HITRAN2020 line lists," J. Quant. Spectrosc. Radiat. Transfer **276**, 107936 (2021). https://doi.org/10.1016/j.jqsrt.2021.107936

21. E. N. Starikova and A. Barbe, "Twelve experimental band centers of the $^{16}O^{16}O^{18}O$ ozone isotopologue in the 3400–5600 cm^{-1} spectral range: Comparison with theoretical predictions from the potential energy surface," Atmos. Ocean. Opt. **35** (2), 103–109 (2022). https://doi.org/10.1134/S1024856022020129

22. D. Mondelain, A. Campargue, S. Kassi, A. Barbe, E. Starikova, M.-R. De Backer, and Vl. G. Tyuterev, "The CW-CRDS spectra of the $^{16}O/^{18}O$ isotopologues of ozone between 5930 and 6340 cm^{-1}. Part 1: $^{16}O^{16}O^{18}O$," J. Quant. Spectrosc. Radiat. Transfer **116**, 49–66 (2013).

23. S. Vasilchenko, A. Barbe, E. Starikova, S. Kassi, D. Mondelain, A. Campargue, and V. Tyuterev, "Detection and assignment of ozone bands near 95% of the dissociation threshold: Ultra-sensitive experiments for probing potential energy function and vibrational dynamics," Phys. Rev. A **102** (5), 052804 (2020).

24. S. S. Vasilchenko, S. Kassi, D. Mondelain, and A. Campargue, "High-resolution laser spectroscopy of the ozone molecule at the dissociation threshold," Atmos. Ocean. Opt. **34** (5), 373–380 (2021).

25. J. C. Depannemaecker and J. Bellet, "Rotational spectra of $^{16}O_3$ and the five ^{18}O isotopic species," J. Mol. Spectrosc. **66**, 106–120 (1977).

26. C. Chiu and E. A. Cohen, "Rotational spectra of mono-^{18}O-substituted ozones in the ν_2 excited vibrational state," J. Mol. Spectrosc. **109**, 239–245 (1985).

27. J. M. Flaud, C. Camy-Peyret, A. N'Gom, V. Malathydevi, C. P. Rinsland, and M. A. H. Smith, "The ν_2 bands of $^{16}O^{16}O^{18}O$ and $^{16}O^{18}O^{16}O$," J. Mol Spectrosc. **133**, 217–223 (1989).

28. P. Roy, J. B. Brubach, M. Rouzieres, O. Pirali, L. Manceron, and Tchana F. Kwabia, "AILES: La ligne IR et THz sur rayonnement synchrotron SOLEIL," Rev. Electricite Electronique **2**, 23 (2008).

29. J. B. Brubach, L. Manceron, M. Rouzieres, O. Pirali, D. Balcon, Tchana F. Kwabia, V. Boudon, M. Tudorie, T. Huet, A. Cuisset, and P. Roy, "Performance of the AILES THz-IR beamline on Soleil for high resolution spectroscopy," AIP Conf. Proc. **1214**, 81–84 (2010).

30. www.synchrotron-soleil.fr/en/beamlines/ailes. Cited September 20, 2023.

31. M. Faye, M. Bordessoule, B. Kanoute, J.-B. Brubach, P. Roy, and L. Manceron, "Improved mid infrared detector for high spectral or spatial resolution and synchrotron radiation use," Rev. Sci. Inst **87**, 063119 (2016).

32. L. Manceron, A. Barbe, V. Tyuterev, B. Grouiez, J. Burgalat, M. Rotger, and P. Roy, "Far infrared spectroscopy of the ozone molecule and its isotopomers between 50 and 800 cm^{-1}," in *Abstracts of the 15th ASA*

Conference (united with 16th HITRAN Conference), Reims, France, August 24–26, 2022. P. 13.

33. V. Tyuterev, A. Barbe, L. Manceron, B. Grouiez, S. Tashkun, J. Burgalat, and M. Rotger, "Ozone spectroscopy in the terahertz range from first high-resolution Synchrotron SOLEIL experiments combined with far-infrared measurements and ab initio intensity calculations," Spectroch. Acta Part A (2023) (in press).
34. J.-J. Plateaux, L. Regalia, C. Boussin, and A. Barbe, "Multispectrum fitting technique for data recorded by Fourier transform spectrometer: Application to N_2O and CH_3D," J. Quant. Spectrosc. Radiat. Transfer **68**, 507–520 (2001).
35. A. Chichery, PhD Thesis (Universite de Reims, 2000).
36. S. A. Tashkun and Vl. G. Tyuterev, "GIP: A program for experimental data reduction in molecular spectroscopy," Proc. SPIE **2205**, 188–191 (1994). https://doi.org/10.1117/12.166203
37. V. Tyuterev, S. Tashkun, M. Rey, and A. Nikitin, "High-order contact transformations of molecular Hamiltonians: General approach, fast computational algorithm and convergence of ro-vibrational polyad models," Mol. Phys. **120,** e2096140 (2022). https://doi.org/10.1080/00268976.2022.2096140
38. J. M. Flaud and R. Bacis, "The ozone molecule: Infrared and microwave spectroscopy," Spectrochim. Acta Part A **54**, 3–16 (1998). https://doi.org/10.1016/S1386-1425(97)00214-X
39. J. M. Flaud and C. Camy-Peyret, "Vibration-rotation intensities in H_2O-type Molecules application to the $2\nu_2$, ν_1, and ν_3 bands of $H_2{}^{16}O$," J. Mol. Spectrosc. **55**, 278–310 (1975). doi 90270-2 https://doi.org/10.1016/0022-2852(75)
40. O. N. Sulakshina, Yu. Borkov, Vl. G. Tyuterev, and A. Barbe, "Third-order derivatives of the dipole moment function for ozone molecule," J. Chem. Phys. **113**, 10572–10582 (2000).
41. J. K. G. Watson, "Determination of centrifugal distortion coefficients of asymmetric-top molecules," J. Chem. Phys. **46**, 4189–4196 (1967).
42. J.-M. Flaud, C. Camy-Peyret, C. P. Rinsland, M. A. H. Smith, and Devi V. Malathy, *Atlas of Ozone Spectral Parameters from Microwave to Medium Infrared* (Academic Press, Boston, 1990).
43. V. G. Tyuterev, R. V. Kochanov, and S. A. Tashkun, "Accurate ab initio dipole moment surfaces of ozone: First principle intensity predictions for rotationally resolved spectra in a large range of overtone and combination bands," J. Chem. Phys. **146**, 064304 (2017). https://doi.org/10.1063/1.4973977